frontiers in Earth Science

ORIGINAL RESEARCH
published: 14 January 2021
doi: 10.3389/feart.2020.590939

Remagnetization of Permian Emeishan basalts: Constraints on the timing of native copper mineralization in northeast Yunnan Province, China

Chengying Liu[1,2]*, *Greig A. Paterson*[3,4], *Shihu Li*[2], *Yongxin Pan*[4] and *Rixiang Zhu*[2]*

[1]Key Laboratory of Mineral Resources in Western China (Gansu Province), School of Earth Sciences, Lanzhou University, Lanzhou, China, [2]State Key Laboratory of Lithospheric Evolution, Institute of Geology and Geophysics, Chinese Academy of Sciences, Beijing, China, [3]Department of Earth, Ocean, and Ecological Sciences, University of Liverpool, Liverpool, United Kingdom, [4]Key Laboratory of Earth and Planetary Physics, Institute of Geology and Geophysics, Chinese Academy of Sciences, Beijing, China

New paleomagnetic results from the Permian Emeishan basalts in the Zhaotong area, NE Yunnan province, China show four natural remanent magnetization components. Detailed stepwise thermal demagnetization of basaltic samples from 16 flows from the Dadi section, which represent basalt units III and IV, isolated two groups of characteristic remanent magnetizations. Samples in unit IV (five flows) record a southwest declination and a moderate downward inclination that is considered to be a partial remagnetized remanence. The bottom flows from unit III (11 flows) record a normal polarity direction, interpreted as a remagnetization, which yields a tilt-corrected mean direction of D_s/I_s = 8.8°/31.6° (N = 9, k_s = 39.7, α_{95} = 8.3°), with a corresponding paleomagnetic pole at 77.1°N, 240.0°E (K = 49.2, A_{95} = 7.4°). The secondary directions have steeper inclinations than primary ones that have been successfully recovered from other studies in this area of the Emeishan basalts. By comparison with the Phanerozoic paleomagnetic poles of the South China Block, the preferred timing of remagnetization is the Lower-Middle Jurassic. Field relationships suggest that the remagnetization of the Emeishan basalts is coeval with the spatially related, but localized, copper mineralization. Thus the timing of the main copper mineralization hosted in the Emeishan basalts is hypothesized to occur in the Early-Middle Jurassic.

Keywords: Emeishan basalts, paleomagnetic study, remagnetization, copper mineralization, Early-Middle Jurassic

OPEN ACCESS

Edited by:
John William Geissman, The University of Texas at Dallas, United States

Reviewed by:
Ann Marie Hirt, ETH Zürich, Switzerland
Marta Neres, Portuguese Institute for Sea and Atmosphere (IPMA), Portugal

***Correspondence:**
Chengying Liu
cyliu@lzu.edu.cn
Rixiang Zhu
rxzhu@mail.igcas.ac.cn

Specialty section:
This article was submitted to Geomagnetism and Paleomagnetism, a section of the journal Frontiers in Earth Science

Received: *03 August 2020*
Accepted: *17 November 2020*
Published: *14 January 2021*

Citation:
Liu C, Paterson GA, Li S, Pan Y and Zhu R (2021) Remagnetization of Permian Emeishan basalts: Constraints on the timing of native copper mineralization in northeast Yunnan Province, China. Front. Earth Sci. 8:590939. doi: 10.3389/feart.2020.590939

INTRODUCTION

The Emeishan flood basalts form a large igneous province (LIP) that covers an area of around 2.5 × 10^5 km^2 in southwestern China, and is considered to have originated from a mantle plume (Xu et al., 2001; He et al., 2003; He et al., 2007). The timing of the Emeishan volcanism has been dated to the Middle to Late Permian (e.g., 259–260 Ma), and is temporally related to the late Guadalupian mass extinction (e.g., Courtillot et al., 1999; Ali et al., 2002; Ali et al., 2005, Ali et al., 2010; Hou et al., 2002; Shellnutt and Jahn, 2011; Shellnutt et al., 2012; Luo et al., 2013; Yan et al., 2013; Li et al., 2018). A series of paleomagnetic studies on the Emeishan basalts have been conducted for more than three decades (McElhinny et al., 1981; Lin et al., 1985; Zhao and Coe, 1987; Van der Voo et al., 1993; Huang and Opdyke, 1998; Zhu et al., 1998; Ali et al., 2002; Liu and Zhu, 2009; Zheng et al., 2010; Liu et al.,

2012). It was noted in early studies that both north-northeast shallow-up (normal) and southwest down (reverse) directions are primary remanent magnetizations (Huang and Opdyke, 1998; Zheng et al., 2010; Liu et al., 2012). However, some researchers have observed that the normal and reverse polarity directions are not antipodal and suggested that some directions are contaminated by unresolved overprinting, with reverse directions more affected than the normal ones (Huang and Opdyke, 1998; Liu et al., 2012). The potential causes of remagnetization, however, have not been established.

There are many traces of copper mineralization and small-volume copper deposits spatially associated with the Emeishan basalts (Zhu et al., 2003; Wang et al., 2006; Li et al., 2009). The Cu concentration of the Emeishan basalts is high (i.e., an average of ~170 ppm) and the copper mineralization grades range from about 1.0 to 4.0 wt% Cu (Zhu et al., 2003; Wang et al., 2010). Since 1958, tens of copper mines have been established in Sichuan, Yunnan and Guizhou provinces (**Figure 1A**). However, none is of significant economic value. A number of studies have suggested that the copper mineralization of the Emeishan basalts was the result of mid-to low-temperature (i.e., <350°C) hydrothermal activity (Wang et al., 2006; Li et al., 2009; Wang et al., 2011). However, the age of copper mineralization remains equivocal. Wang et al. (2006) suggested that either Triassic magmatism or hydrothermal activity at ~230 Ma is associated with the copper deposits, whereas, Li et al. (2009) suggested that the main copper mineralization phase was during the Middle to Late Jurassic. Ar^{39}-Ar^{40} whole-rock dating on basalt sample from the Emeishan

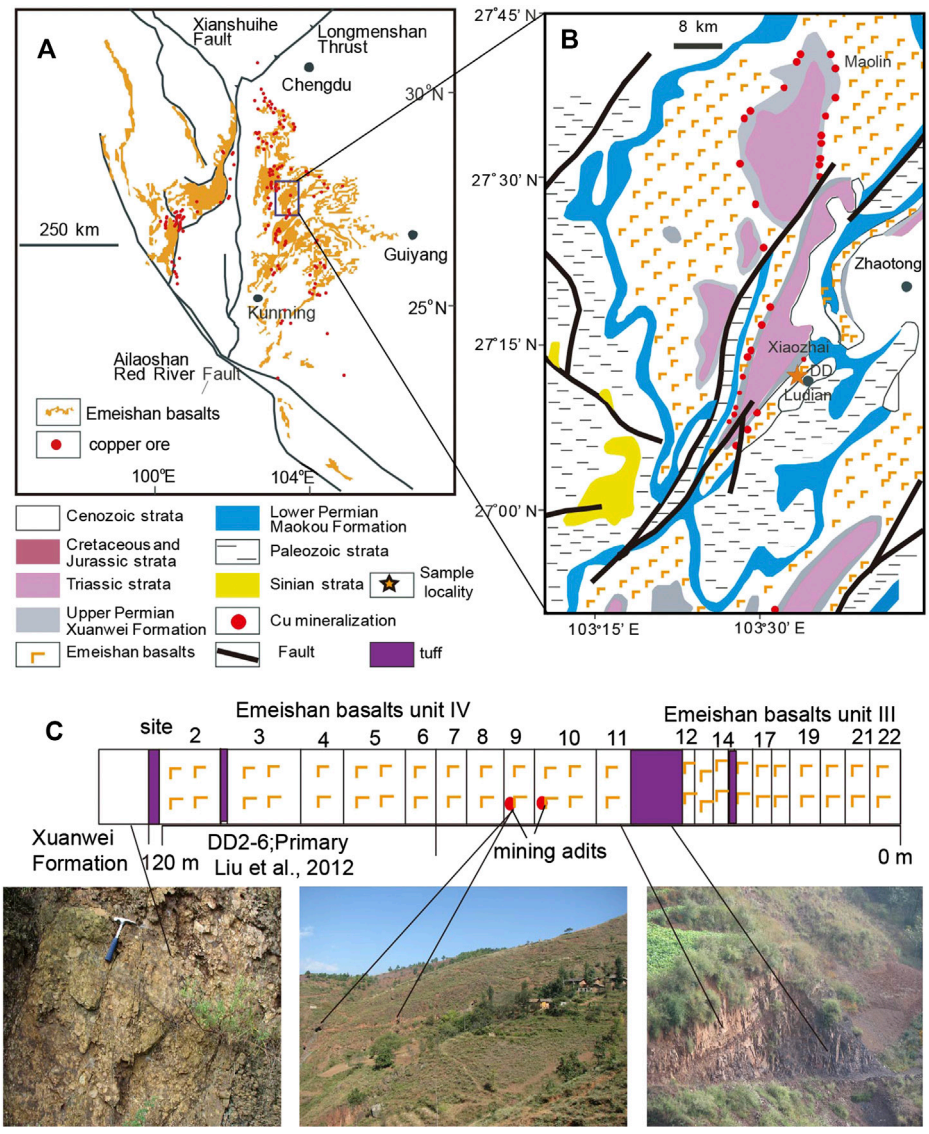

FIGURE 1 | (A) The distribution of the Emeishan basalts and cooper ore in southwest China (after Li et al., 2009) **(B)** Geologic map of the Zhaotong area, Yunnan Province, showing the distribution of copper mineralization localities (after Wang et al., 2006) and the sample locality (DD) **(C)** The lithology column of Dadi section and typical outcrop pictures.

basalts yield a range of Mesozoic and Cenozoic overprint cooling ages (Hou et al., 2002; Ali et al., 2004). However, the relationship between copper mineralization, the Ar^{39}-Ar^{40} overprint ages and paleomagnetic doubts from the Emeishan basalts is unclear.

This paper presents new paleomagnetic results from the Emeishan basalts from the Dadi section in the Zhaotong area, northeast Yunnan province. This section is associated with native copper deposits and data from this region allows us to obtain the timing of copper mineralization.

GEOLOGIC SETTING AND SAMPLING

The Emeishan basalts are exposed across large parts of Yunnan, Sichuan and Guizhou provinces in southwest China (**Figure 1A**). The main body of the Emeishan LIP (ELIP) is bounded by the Longmenshan-Xiaoqinghe faults to the north-northwest and the Ainaoshan-Honghe faults to the southwest (He et al., 2003; Liu and Zhu, 2009; **Figure 1A**). The basalt sequences range in thickness from 1.0 to 5.0 km in the west to several hundred meters in the east (Ali et al., 2005). A mantle plume head located in the western part of Binchuan–Miyi area, northwest of Kunming has been suggested to explain these thickness variations (Xu et al., 2004; He et al., 2007). The Emeishan basalt sequences in northeast Yunnan province are usually over 1,000 m thick. In this area, the basalts unconformably overlie the Middle Permian Maokou Formation and are unconformably overlain by the Upper Permian Xuanwei Formation. The Maokou Formation is mainly comprised of fossiliferous marine limestone (Wang and Van der Voo, 1993). The Xuanwei Formation is composed of continental deposits of sandstones, mudstones, thin coal seams with basal conglomerates in the northern parts (Yunnan Bureau, 1989). The Emeishan basalt sequence in this area is divided into four stratigraphic units, I–IV up section (Wang et al., 2006; Liu et al., 2012). After the eruption of the Emeishan basalt, the most significant magmatic activity in this area was in the Late Triassic (Yunnan Bureau, 1989; Li et al., 2009). Regional faults mostly with a northeast strike (**Figure 1B**), are part of the Mesozoic shortening belt system within the Yangtze China Block that resulted from the Yanshanian Movement (Yang et al., 1986; Yan et al., 2003; Li et al., 2009; Dong et al., 2015). Copper mineralization is largely concentrated in unit IV of the Emeishan basalts, which are generally 50–100 m thick and composed of 3–5 distinct basalt flows. The copper ore bodies and mineralization bodies, tens of centimeters to 2 m thick, mainly are located in schistose amygdaloidal basalt, amygdaloidal basaltic breccias and carbonaceous sedimentary rocks between of different basalt flows. The footwall and hanging wall of the ore bodies are generally massive basalt (Li et al., 2009). The native copper deposits in the northeast Yunnan province are mainly distributed along the limbs of the Xiaozhai and Maolin synclines (Wang et al., 2006; Li et al., 2009; **Figure 1B**). The northwest limb of the Xiaozhai syncline dips at 30–48°S and the southeast limb dips at 20–37°N (Wang et al., 2006). All of the copper mines in northeast Yunnan province are of limited scale or only have small Cu mineralization. For instance, the estimated reserve of one occurrence on the southeast limb is 16,000 tons of Cu mineralization at an average grade of 1.5 wt% Cu with a strike length about 500 m and an average thickness of 10 m (Zhu et al., 2003).

The basalt section in the Zhaotong area, northeast Yunnan province, was sampled near the village of Dadi (DD; 27.22°N, 103.54°E; **Figure 1B**). The total sampled sequence at Dadi section is ~140 m, containing a thick conglomerate bed (~5 m) of the Upper Permian Xuanwei Formation and at least 21 flows, each ranging from 1 to 12 m (**Figure 1C**). Unit III of the Emeishan basalts forms the base of this section and a tuff layer separates units III and IV of the basalts (**Figure 1C**). The upper part of the section is overlain by conglomerate bed of the Xuanwei Formation (**Figure 1C**). The contact between unit IV of the basalts and the conglomerate is a parallel, unconformable boundary. The paleomagnetic directions recorded in the basaltic cobbles from the Xuanwei Formation conglomerate pass a conglomerate test, suggesting that the magnetization in the underlying Emeishan basalts is primary (Liu et al., 2012). The upper parts of the unit IV basalts (sites DD2-6; ~50 m; **Figure 1C**) have been studied by Liu et al. (2012) and record a southwest shallow downward (reverse) direction, which is consistent with the reverse polarity magnetization elsewhere in the ELIP. The focus in this study is on the underlying sixteen flows, including the lower eleven basalt flows (sites DD12–22, each 1–5 m thick), mid-basalt tuffs (~8 m) and five upper basalt flows (sites DD7-11, each 5–10 m thick) sampled in this study. The ~8 m purple-red tuff marks the boundary between basalt unit III and unit IV (Yunnan Bureau, 1989; **Figure 1C**). Sites DD7-11 are part of unit IV and were separated by a ~3 m rivulet from sites DD2-6, that is labeled as a fault in **Figure 1C**. Sites DD12–22 belong to unit III. The basalt unit III in adjacent Shuimo (SM) section in Zhaotong area yields primary northeast and shallow up (normal) directions (Liu et al., 2012). The individual basalt flows grade from massive, to vesiculated, to brecciated from bottom to top. Four abandoned mining adits are visible, two are within the DD9 and DD10 flows (Unit IV) near the sample sites and two others were ~1 km from the sampled section in the flows DD14 and DD17 (Unit III).

A total of 176 oriented samples were taken from the sixteen flows using a handheld petrol drill with water cooling. Both magnetic and sun compasses were used for *in-situ* core orientation, and less than 5° difference was found between the two orientations. Samples were further processed in the laboratory into specimens (generally 0.5 cm height cylinder to reduce the intensity with the diameter of 2.54 cm) suitable for paleomagnetic measurements. Fresh off-cuts were used for rock magnetic and microscope investigations.

METHODS

All specimens were subjected to progressive thermal demagnetization in 13–15 steps up to 550 or 585°C using an ASC TD–48 oven in a magnetically shielded room (residual field <300 nT). The remanence was measured using a 2G Enterprises 755R SQUID magnetometer. The magnetic component

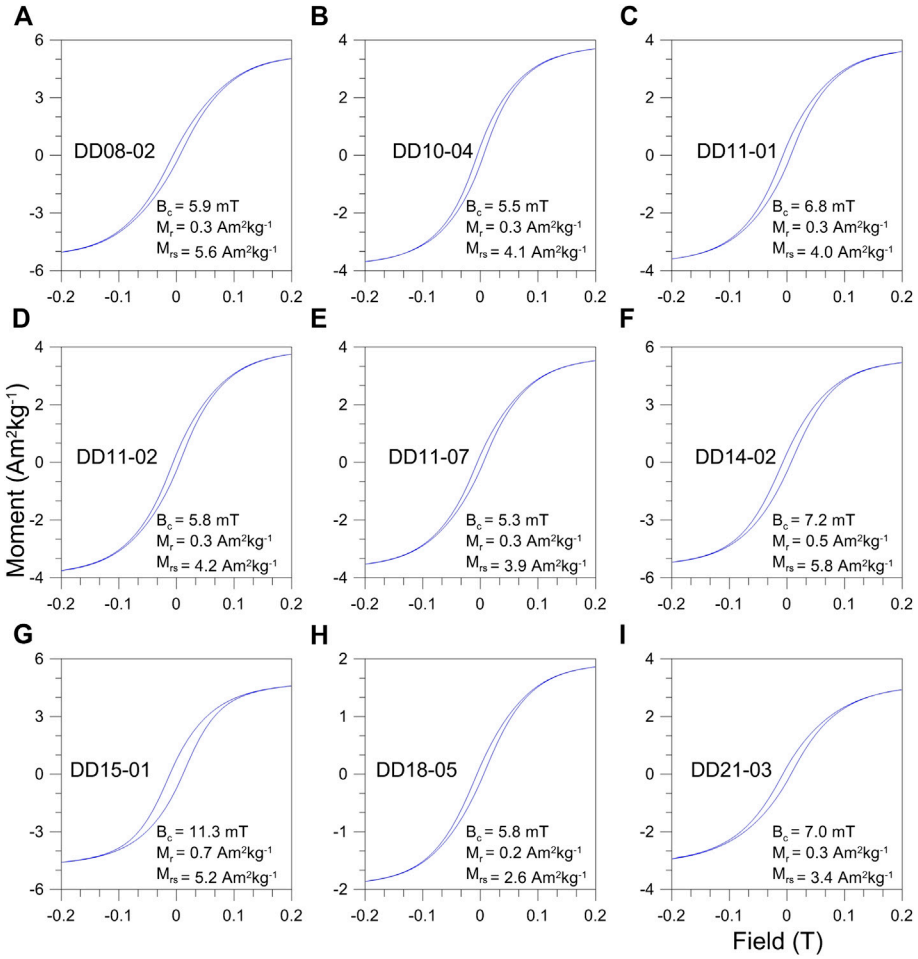

FIGURE 2 | Representative hysteresis loops of basalt samples at the Dadi section. The saturation field is ±1 T. B_c, coercivity; M_r, remanent magnetization; M_{rs}, saturation magnetization.

directions were determined using principal component analysis (Zijderveld, 1967; Kirschvink, 1980) as implemented by the PaleoMag software using linear fitting (Jones, 2002) or great circle fitting by using PMGSC software. All data fits were made using at least four points. To compare with the thermal demagnetization behavior, 24 sister samples were subjected to stepwise alternating field (AF) demagnetization with eleven steps up to 80 mT using a 2G–760R long-core SQUID magnetometer with an inline AF demagnetization system. In most cases, however, AF demagnetization does not fully resolve the paleomagnetic directions, therefore only the thermal demagnetization results are used for further analysis. Fisher statistics (Fisher, 1953) were used to compute the site mean directions and the equal area projections of the directions were analyzed and plotted with the PmagPy software (Tauxe, 2010). The same attitude of the stratum (strike/dip = 357°/20°) for the upper sites DD2-6, which was measured from the overlying Xuanwei Formation sediments (Liu et al., 2012), is used for all tilt corrections.

To characterize the composition and domain state of the magnetic carriers, 27 hysteresis loops were measured on a Princeton Measurement MicroMag 3,900 Vibrating Sample Magnetometer (VSM3900) at room temperature with a field range of ±1 T. Isothermal remanent magnetization (IRM) acquisition up to 1 T and backfield demagnetization to −0.5 T of representative specimens were also conducted on the VSM3900 and the coercivity components of each specimen were analyzed (Kruiver et al., 2001). The hysteresis parameters are plotted on a Day-plot (Day et al., 1977; Dunlop, 2002). The temperature dependence of susceptibility was measured in air from room temperature to 700°C using an AGICO MFK1 Kapabridge equipped with a CS-3 high-temperature furnace in a field of 200 A/m at a frequency of 976 Hz. To investigate the micro-texture of the basaltic samples directly, polished thin sections were studied by reflected light microscope. All paleomagnetic and magnetic measurements were performed in the Paleomagnetism and Geochronology Laboratory of the Institute of Geology and Geophysics, Chinese Academy of Sciences.

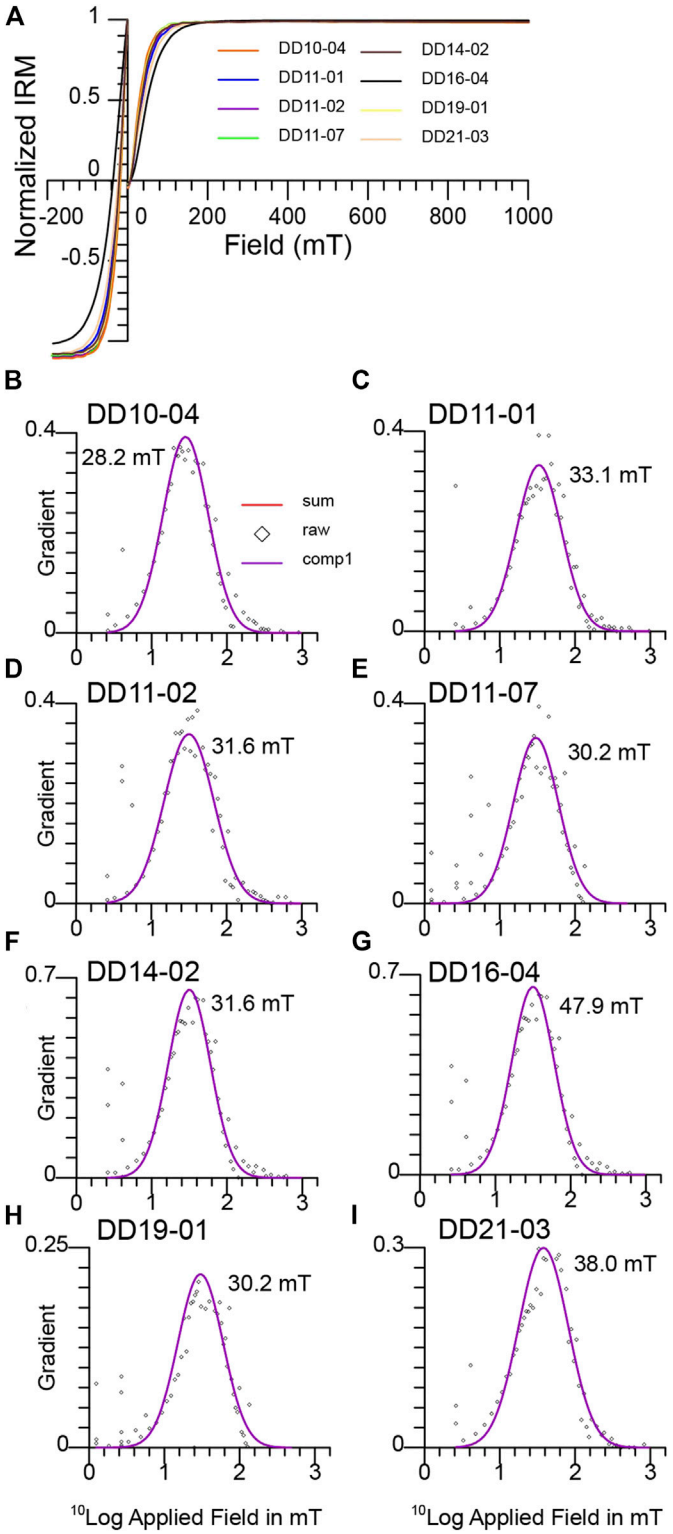

FIGURE 3 | (A) IRM acquisition curves of representative samples **(B–I)** IRM decomposition curves of these samples.

TABLE 1 | Values of midpoint $B_{1/2}$ of the IRM components.

Sample	Comp	Contri (%)	$B_{1/2}$ (mT)	DP (mT)
DD08-01	1	100	35.5	0.30
DD08-02	1	100	39.8	0.30
DD08-04	1	100	26.3	0.30
DD08-05	1	100	38.9	0.32
DD08-06	1	100	28.8	0.30
DD09-02	1	100	29.5	0.30
DD10-04	1	100	28.2	0.30
DD10V06	1	100	28.2	0.30
DD10-12	1	100	50.1	0.28
DD10-14	1	100	41.7	0.30
DD10-16	1	100	31.6	0.30
DD10B-4	1	100	27.5	0.33
DD11-01	1	100	33.1	0.30
DD11-02	1	100	31.6	0.33
DD11-03	1	100	30.2	0.28
DD11-05	1	100	42.7	0.28
DD11-07	1	100	30.2	0.30
DD11-10	1	100	30.9	0.28
DD13-06	1	100	31.6	0.29
DD14-02	1	100	31.6	0.28
DD15-01	1	100	34.7	0.26
DD16V04	1	100	47.9	0.28
DD17-01	1	100	35.5	0.35
DD18-05	1	100	22.4	0.35
DD19-01	1	100	30.2	0.30
DD20-05	1	100	28.8	0.36
DD21-03	1	100	38.0	0.33
Average			33.5 ± 6.5	

RESULTS

Rock Magnetism

The room temperature hysteresis loops of specimens from the flows DD7-22 are closed by ≤ 0.2 T and have low coercivity (H_c) values range from 3.8 to 11.7 mT with a mean of 6.4 ± 2.2 mT (n = 27; **Figure 2**). The saturation magnetizations (M_s; acquired at 1 T) range from 2.4 to 6.0 Am^2kg^{-1}, with saturation remanence (M_{rs}) values (0.2–0.6 Am^2kg^{-1}).

The IRM acquisition curves indicate that the specimens reach >95% saturation in fields of ~0.2 T (**Figure 3**). The back-field demagnetization indicates that remanence coercivity (H_{cr}) is generally less than 30 mT, with average of 20.9 ± 4.8 mT (n = 27). There is single coercivity component with coercivity midpoint ($B_{1/2}$) range from 22.4 to 50.1 mT, with a mean of 33.5 ± 6.5 mT of conducted samples (**Figure 3**; **Table 1**).

Temperature dependent susceptibility of representative samples from unit IV and III sharply drops at ~585°C (**Figure 4**). All together the rock magnetism strongly suggests that (low-Ti) magnetite is the dominant magnetic carrier for the flows from Units III and IV on this section.

The M_{rs}/M_s vs. H_{cr}/H_c value on the Day-plot show that the bulk magnetic properties of the DD7-22 samples fall into the pseudo-single-domain region and generally follow the single domain (SD) and multidomain (MD) mixing curves, suggesting mixtures of SD and MD magnetite grains (Day et al., 1977; Dunlop, 2002; **Supplementary Figure S1**).

Paleomagnetic Directions

The lava flows are classified into two groups according to their stratigraphic units sampled. Unit III is comprised of flows DD12 to DD22 (106 samples) and unit IV is comprised of flows DD7 to DD11 (70 samples). The demagnetization diagrams for representative samples are shown in **Figures 5**, **6** and the paleodirections are summarized in **Figure 7** and listed in **Tables 2**, **3**.

For unit III specimens, one or two components can be isolated from the demagnetization trajectories (**Figure 5**). A low-temperature component (referred to as III-1) is separated below ~300°C in 85 out of 106 unit III specimens with maximum angular deviation (MAD) less than 15°. Eleven outliers were further rejected for inclusion in the means, including ten directions with geographic declination (D_g) range from 90° to 270°, with positive inclinations and one with negative inclinations. The final calculated mean directions of III-1 components is D_g/I_g = 10.6°/45.8° (n = 74, k_g = 11.1, α_{95} = 4.9°) and 13.7°/46.0° (N = 9, n = 74, k_g = 63.3, α_{95} = 5.9°) on specimen and site level, respectively. These two mean directions are similar at the 95% CI. The latter one corresponds to a geomagnetic pole of 77.8°N, 187.8°E (N = 9, K_g = 56.7, A_{95} = 6.2°) and is used for further discussion (**Table 2**; **Figure 7A**). After tilt correction, the mean direction of III-1 component is D_s/I_s = 352.0°/48.1° (N = 9,

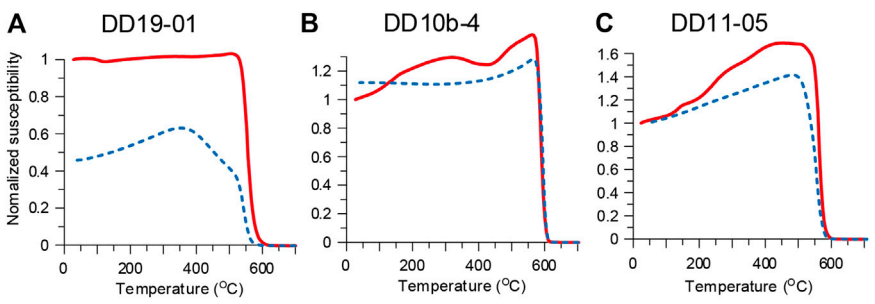

FIGURE 4 | Representative temperature dependent magnetic susceptibility for samples from unit III **(A)** and unit IV **(B,C)**. Bold/dashed lines indicate the heating/cooling curves.

k_s = 63.2, α_{95} = 5.9°) that corresponds to a geomagnetic pole of 82.6°N, 33.7°E (N = 9, K_s = 52.3, A_{95} = 6.5°).

After removal of the low-temperature component, the characteristic remanent magnetization (ChRM) component of unit III specimens (III-2) can be isolated between ~350–420°C and 585°C by a well-defined linear segment decaying to the origin on the orthogonal vector diagrams with MAD less than 10° (**Figure 5**). The site mean III-2 direction is D_g/I_g = 19.4°/25.6° (N = 9, n = 81; k_g = 39.7, α_{95} = 8.3°) before and D_s/I_s = 8.8°/31.6° (N = 9, n = 81; k_s = 39.7, α_{95} = 8.3°) after tilt correction. This corresponding to a geomagnetic pole of 67.2°N, 226.0°E (K_g = 42.2, A_{95} = 8.0°) and 77.1°N, 240.0°E (K_s = 49.2, A_{95} = 7.4°), respectively (**Table 3**; **Figure 7D**).

Demagnetization behavior of the unit IV specimens is more complicated. In general, a component with low unblocking temperature (IV-1), up to ~300°C, can be isolated from most samples (**Figures 6A,B**), generating similar mean directions of D_g/I_g = 5.8°/41.6° (n = 60; k_g = 14.1, α_{95} = 4.8°) and 6.5°/41.0° (N = 4; n = 60; k_g = 61.7, α_{95} = 11.8°) on specimen and site level, respectively. The latter one is used for further discussion and corresponds to a geomagnetic pole of 85.9°N, 181.7°E (N = 4, K_g = 63.9, A_{95} = 8.8°; **Table 2**). In some cases, the unblocking temperature of IV-1 component is as high as ~500°C and overlaps with the ChRM component (IV-2, **Figures 6C,D**). The IV-2 component, which has unblocking temperatures of ~500°C–580°C, can only be isolated from few specimens (five out of 70) from site DD10 using linear fit method (**Figures 6A,B**) and in most cases overlaps with the IV-1 component. This behavior is revealed in vector component diagrams as curved demagnetization trajectories and on equal-area diagrams as great circles (**Figures 6C,D**). A combined analysis of remagnetization great circles and directions using the method of McFadden and McElhinny (1988) yields a mean of D_g/I_g = 195.1°/31.2° (n = 22, k_g = 32.9, α_{95} = 11.9°) and D_s/I_s = 196.7°/27.9° (n = 22, k_s = 50.1, α_{95} = 9.6°) before and after tilt correction, which correspond to virtual geomagnetic pole (VGP) at 43.6°N,263.4°E and 44.9°N, 260.4°E, respectively (**Table 3**; **Figure 7C**).

Mineralogy Inspection

Two representative specimens, DD10-10 from unit IV and DD21-03 from unit III, were investigated using optical microscopy. The two samples both have a fine matrix with a predominance of plagioclase microphenocrysts (**Figures 8A–F**). Interspersed pyroxene and other opaque minerals with a small amount of olivine are also observed (**Figures 8C,F**). The grain size of the plagioclase laths ranges from 0.05 to 0.2 mm and the pyroxene has variably altered to chlorite (**Figures 8B,C,E,F**). The amygdales found with the vesicles of DD21-03 are composed of chlorite and zeolite (**Figures 8E,F**), which are commonly the result of epithermal alteration (Wei and Powell, 2003). Compared with the specimens in the upper flows, which record a primary remanence (sample DD4-03; **Figures 8G–I**), a higher amount of chlorite is observed in specimens DD10-10 and DD21-03 in this study. The higher degree of chlorite formation suggests that flows DD7-22 may have experienced a higher degree of hydrothermal alteration.

DISCUSSION

Nature of Magnetization

The Fisher mean of the accepted IV-1 *in-situ* directions of D_g/I_g = 6.5°/41.0° (N = 4; k_g = 61.7; α_{95} = 11.8°) and tilt corrected values of 348.8°/41.3° (N = 4; k_s = 61.3; α_{95} = 11.8°) (**Table 2**; **Figure 7A**).

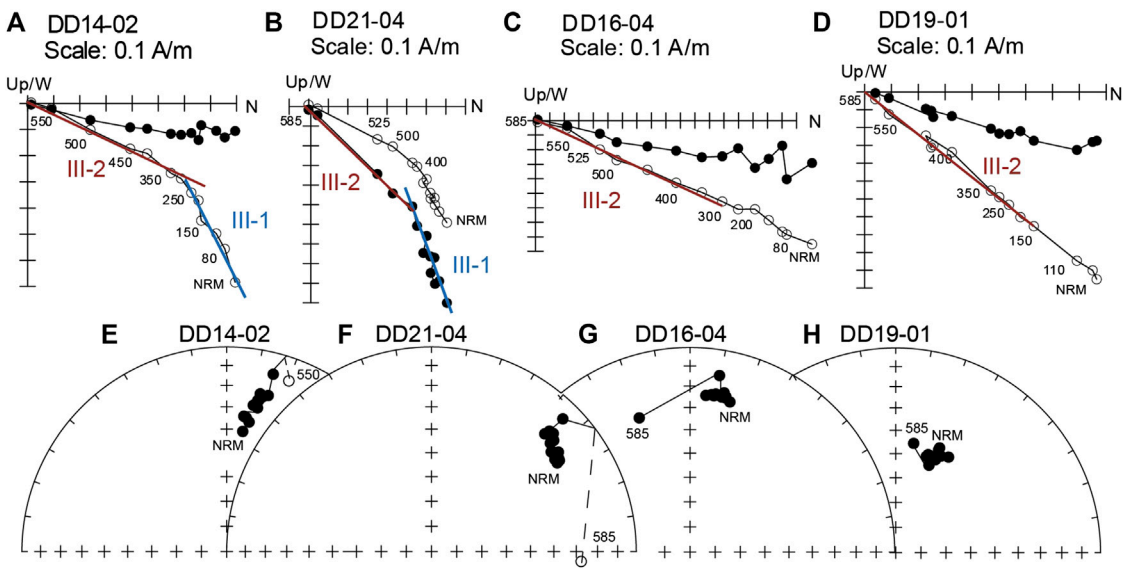

FIGURE 5 | (A–D) Representative orthogonal plots (Zijderveld, 1967) of stepwise thermal demagnetization behavior of Emeishan basalt unit III. Open (solid) circles represent projections on to vertical (horizontal) plane **(E–H)** Equal-area projections of the thermal demagnetization directions. Open (solid) circles represent lower **(upper)** hemisphere projection. The numbers indicate the thermal demagnetization levels in °C.

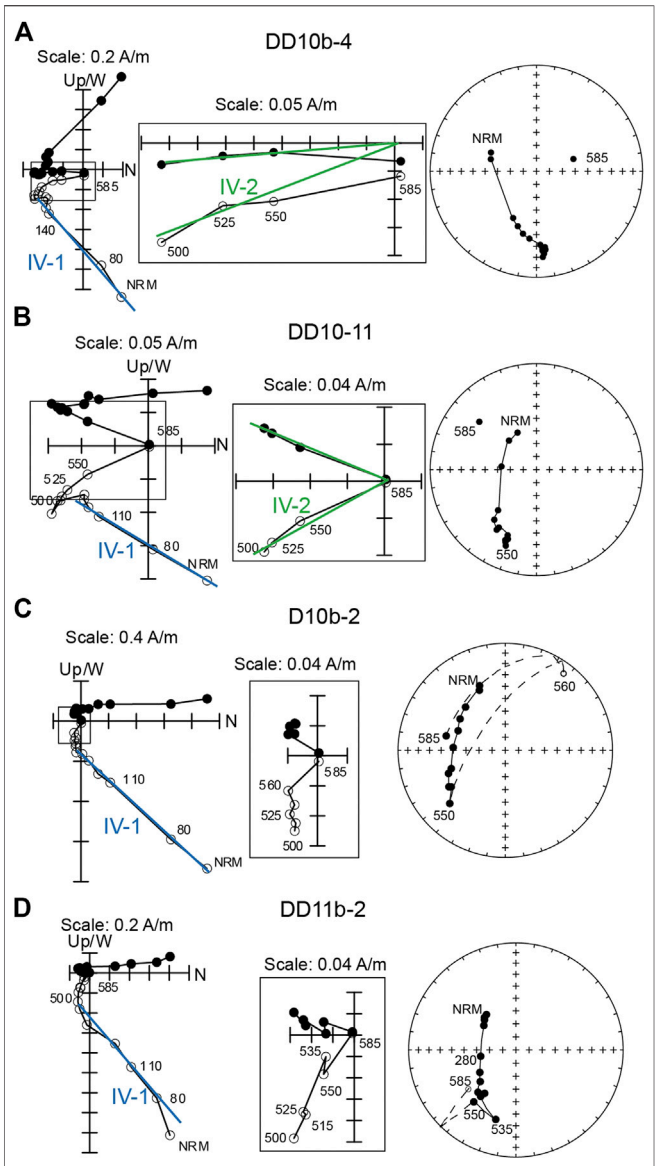

FIGURE 6 | (A–D) Representative orthogonal plots (Zijderveld, 1967) of stepwise thermal demagnetization behavior of Emeishan basalt unit IV. Symbols are the same as in **Figure 6**.

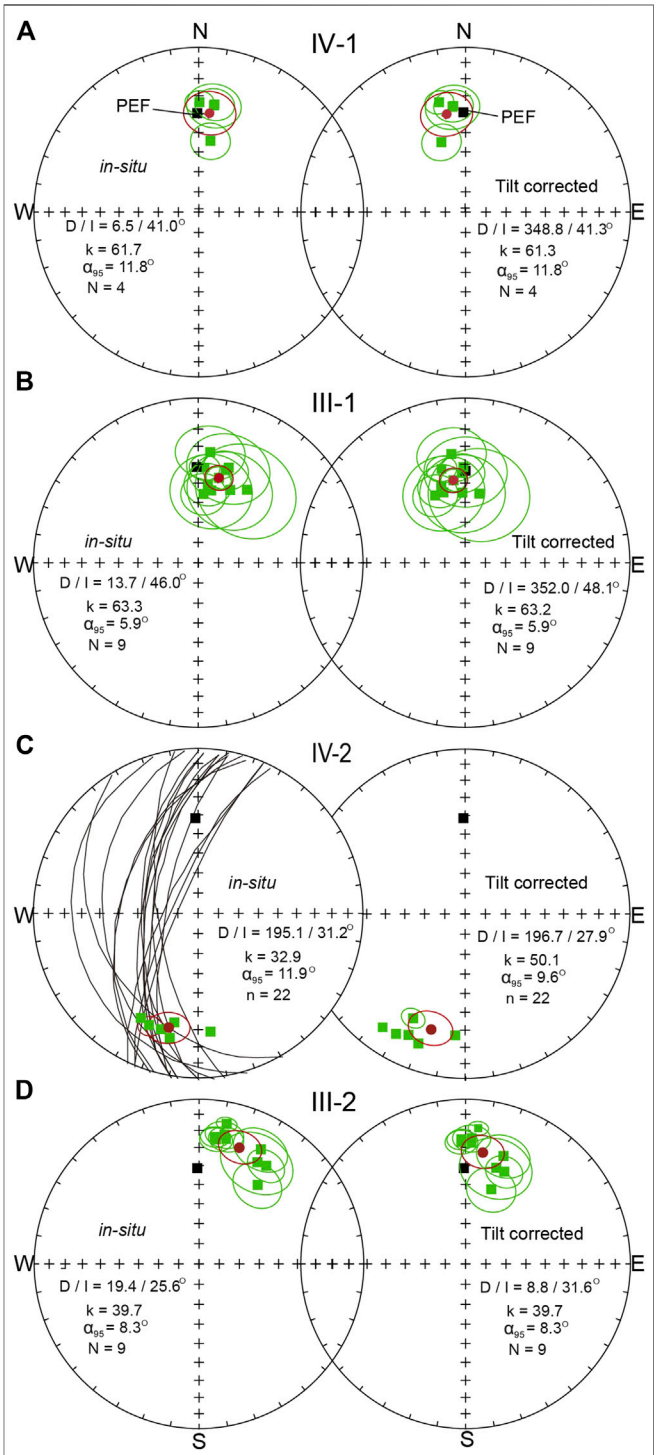

FIGURE 7 | Equal-area projections of paleodirections before and after tilt correction. PEF: present Earth's magnetic field direction (black square). The ellipses indicate the 95% confidence level about the specimen-mean direction (green square) or site-mean direction (red dot).

These mean directions are all near identical to the present Earth field (PEF) direction (D/I = 359.0°/41.5°; **Figure 7A**), which suggested that IV-1 components are recent geomagnetic overprints.

The mean directions of III-1 components are 13.7°/46.0° (N = 9; k_g = 63.3; α_{95} = 5.9°) and 352.0°/48.1° (N = 9; k_s = 63.2; α_{95} = 5.9°) before and after tilt correction, respectively (**Table 2**; **Figure 7B**). This is close to, but different from PEF (**Figure 7B**). The corresponding geomagnetic pole of component III-1 in geographic/strata coordinates is (77.8°N, 187.8°E) and (82.6°N, 33.6°E), respectively (**Table 2**; **Figure 9B**). Comparing this to the apparent polar wander path (APWP) of the South China Block, these poles are identical to the Paleogene- Quaternary (E-Q) and Upper Cretaceous (K_2) poles in the 95% CI, respectively (Huang et al., 2008; Huang et al., 2018 and references therein; **Figure 9B**). If both directions were accepted, it suggests that

TABLE 2 | Paleomagnetic directions and statistics of low temperature components (IV-1 and III-1) from sites DD7-22 at the Dadi section.

Site	n/N	D_g (°)	I_g (°)	k_g	α_{95g} (°)	D_s (°)	I_s (°)	k_s	α_{95s} (°)	Lat. (°N)	Long. (°E)	K	A_{95}(°)
Component IV-1													
DD8[a]	12/15	8.6	36.1	20.9	8.8	353.5	37.5	20.9	8.8				
DD9	12/12	8.3	36.7	11.2	12.1	352.9	38.0	11.2	12.1				
DD10	19/22	0.3	35.6	25.4	6.4	346.2	34.2	25.3	6.4				
DD11	17/21	9.7	55.7	13.1	9.4	340.2	55.0	13.1	9.4				
Mean	4	6.5	41.0	61.7	11.8					85.9	181.7	63.9	8.8
						348.8	41.3	61.3	11.8	79.2	0.1	73.2	8.2
Component III-1													
DD12	12/12	3.8	41.7	33.8	6.9	345.9	40.9	33.8	6.9				
DD13	13/14	4.3	55.6	13.2	10.7	336.0	53.1	13.2	10.7				
DD14	10/13	7.0	50.4	15.8	11.1	342.8	49.6	15.9	11.1				
DD17[a]	12/30	6.2	33.0	7.1	15.2	352.8	33.9	7.1	15.2				
DD18	5/5	16.5	41.0	36.0	10.4	358.0	44.6	36.0	10.4				
DD19	6/12	23.7	50.1	8.0	20.2	357.8	55.0	8.0	20.2				
DD20	6/6	10.2	53.3	10.4	19.4	342.9	53.2	10.4	19.4				
DD21	5/8	33.7	45.8	6.7	24.1	11.6	54.7	6.7	24.1				
DD22	6/6	17.8	39.3	9.1	18.9	0.3	43.5	9.1	19.0				
Mean	9	13.7	46.0	63.3	5.9					77.8	187.8	56.7	6.2
						352.0	48.1	63.2	5.9	82.6	33.7	52.3	6.5

Notes: n/N, numbers of the chosen/conducted samples or site; D_g (D_s), I_g (I_s), declination and inclination before (after) tilt correction; k/K, Fisher statistic precision parameter of the mean direction/poles; α_{95}, radius of the 95% confidence circle about the mean direction; Lat/Long, the longitude/latitude of the paleomagnetic pole or the virtual geomagnetic pole in stratigraphic coordinates; A_{95}, the 95% confidence circle about the paleomagnetic pole.

[a]*Indicates the site-mean direction is combined by adjacent flows.*

the folding occurred after the Upper Cretaceous, which is contradicts current theories (Yang et al., 1986; Yan et al., 2003; Li et al., 2009; Dong et al., 2015). Furthermore, the Fisher statistic precision parameter of the mean direction before (k_g) and after (k_s) tilt-correction is equal that indicates the tilt correction is invalid (Van der Voo, 1990). Therefore, the *in-situ* III-1 directions are preferred, which suggests that the III-1 represent viscous remanent magnetization acquired during Paleogene to Quaternary period.

The mean direction of IV-2 component has a southwest declination and a moderate down inclination (D_g/I_g = 195.1°/31.2°, n = 22, k_g = 32.9, α_{95} = 11.9°; D_s/I_s = 196.7°/27.9°, n = 22, k_s = 50.1, α_{95} = 9.6°; **Table 3**; **Figure 7C**). The $k_s/k_g > 1.5$, indicating the tilt-corrected directions were better clustered that suggest the IV-2 components were obtained before folding. The tilt-corrected IV-2 mean directions are roughly equal to the primary remanence obtained from our previous work in this area where a mean reverse polarity direction of D_s/I_s = 205.9°/10.0° (N = 5, k_s = 78.4, α_{95} = 8.7°; **Figure 9A**) was obtained from the upper flows from this section (Liu et al., 2012). Comparison of the mean directions of IV-2 to the primary ones reveals an angular difference of ~19°, although this bias is significant, it is likely due to contamination by unresolved overprints in the new data, as evidenced by the need to use great circles. The VGP generated from IV-2 components is close to late Permain poles and far away from any younger poles (Huang et al., 2008; Huang et al., 2018 and references therein; **Figure 9B**). From this we infer that unit IV basalts have experienced a significant partial remagnetization event.

The mean declinations of component III-2 (D_g/D_s = 19.4°/8.8°) is broadly similar to the normal direction recovered from the SM section investigated by Liu et al. (2012) (D_s/I_s = 11.0/-5.2°, N = 12, k_s = 53.7, α_{95} = 6.0°). The inclination of the III-2 component (I_g/I_s = 25.6°/31.6°), however, is much steeper (**Figure 9A**). The corresponding paleomagnetic pole before and after tilt correction of the III-2 component is (67.2°N, 226.0°E; K = 42.2, A_{95} = 8.0°) and (77.1°N, 240.0°E; K = 49.2, A_{95} = 7.4°), respectively (**Table 3**). When compared to the APWP of the South China Block, the poles generated from III-2 components lies distinct from Permian poles (**Figure 9B**). The III-2 geomagnetic poles before and after tilt correction fall within the 95% confidence ellipsoids of Late Jurassic (J_3) and Middle-Early (J_{1-2}) poles, respectively (Huang et al., 2008; Huang et al., 2018 and references therein; **Figure 9B**). This observation is unlikely to be the result of paleosecular variation (PSV). Langereis et al. (2012) undertook a PSV analysis of the Permo-Carboniferous Reverse Superchron (PCRS), which ended at ~263 Ma, shortly before the emplacement of the ELIP. They found that PSV during the PCRS was comparably low to that found during the Cretaceous Normal Superchron (Biggin et al., 2008), but distinctly lower than more recent time periods. From our eleven lava flows we calculate a VGP scatter value of 11.3° and that from 30 flows at the SM section and upper five flows at the DD section is 10.8° and 9.2° (at an equatorial paleolatitude), respectively (Liu et al., 2012), which is comparable to the equatorial values from both superchrons. This suggests that PSV immediately after the PCRS remained low and is unlikely to explain the observed difference in pole positions from our data. We conclude that our III-2 directions correspond to an overprint.

The F-test (Butler, 1992) confirms that the geomagnetic poles before and after tilt correction of III-2 components are consistency with J_3 (67.4°N, 218.8°E; K = 78.0, A_{95} = 7.6°; N = 6; calculated from data listed in Huang et al., 2018 and references therein) and J_{1-2} poles (79.1°N, 226.9°E; A_{95} = 4.5°; Yang and

TABLE 3 | Paleomagnetic directions and statistics of ChRM (IV-2 and III-2) from sites DD7-22 at the Dadi section.

Site	n/N	D_g (°)	I_g (°)	k_g	α_{95g} (°)	D_s (°)	I_s (°)	k_s	α_{95s} (°)	Lat. (°N)	Long. (°E)	K	A_{95}(°)
Component IV-2													
Mean_Linear	5	195.2	27.4	46.4	11.4	203.4	19.8						
Mean_GC	17	194.3	34.1	50.3	5.3	206.7	29.7						
Mean	22	195.1	31.2	32.9	11.9					43.6	263.4		
						196.7	27.9	50.1	9.6	44.9	260.4		
Component III-2													
DD12	12/12	12.3	23.5	30.4	7.3	2.9	27.3	30.4	7.3				
DD13	13/14	7.8	24.7	31.8	6.9	358.1	26.8	31.8	6.9				
DD14	10/13	7.2	23.3	54.7	6.0	358.1	25.3	54.7	6.0				
DD16[a]	10/14	11.2	14.4	116.6	4.1	5.4	18.3	116.7	4.1				
DD17	9/16	11.2	21.1	34.6	7.9	2.8	24.6	34.6	7.9				
DD18	5/5	36.6	40.0	29.0	11.6	19.1	50.4	29.0	11.6				
DD19	8/12	34.4	28.5	33.9	8.5	22.8	39.1	33.8	8.5				
DD20	5/6	29.9	29.5	14.5	16.4	17.7	38.6	14.5	16.4				
DD22[a]	9/14	28.4	22.0	15.5	11.8	19.4	31.1	15.6	11.8				
Mean	9	19.4	25.6	39.7	8.3					67.2	226.0	42.2	8.0
						8.8	31.6	39.7	8.3	77.1	240.0	49.2	7.4

Notes: n/N, numbers of the chosen/conducted samples or site; D_g (D_s), I_g (I_s), declination and inclination before (after) tilt correction; k/K, Fisher statistic precision parameter of the mean direction/poles; α_{95}, radius of the 95% confidence circle about the mean direction; Lat/Long, the longitude/latitude of the paleomagnetic pole or the virtual geomagnetic pole in stratigraphic coordinates; A_{95}, the 95% confidence circle about the paleomagnetic pole.

[a]*Indicates the site-mean direction is combined by adjacent flows.*

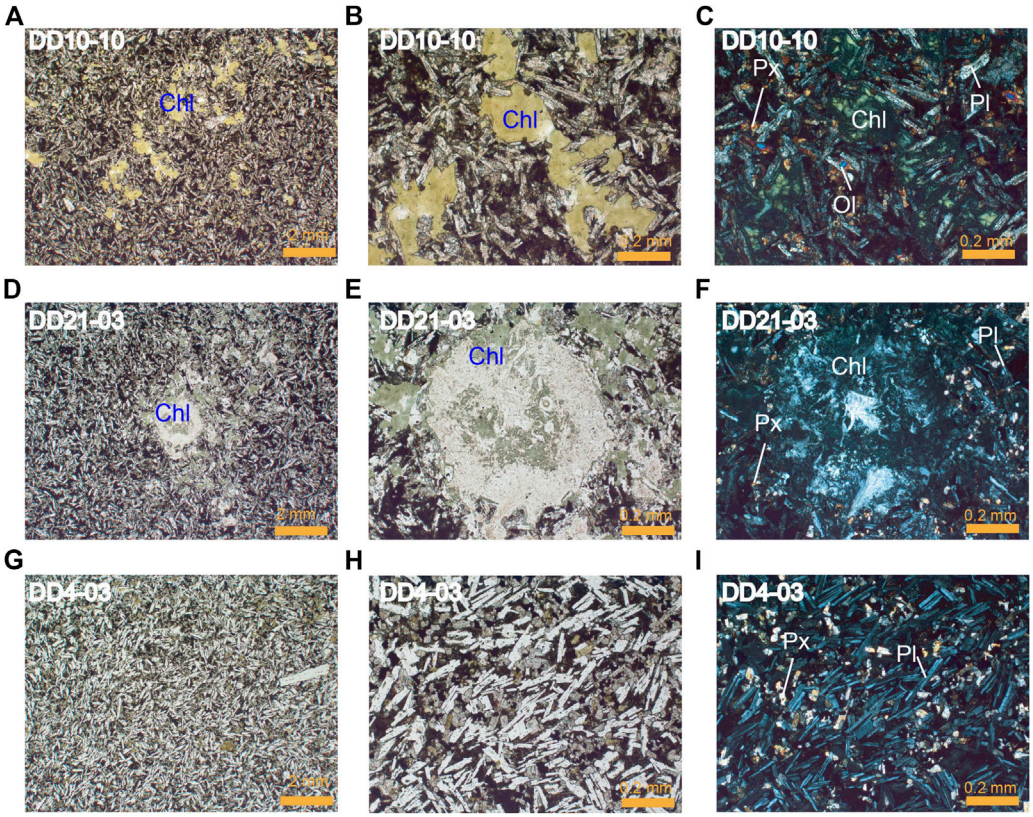

FIGURE 8 | Microphotographs from basaltic sample DD10-10 from unit IV **(A–C)**; sample DD21-03 from unit III **(D–F)** in this study and **(G–I)** sample DD4-03 which carries a primary remanence **(G F I)** are in cross-polarized light and the others in plane-polarized light.

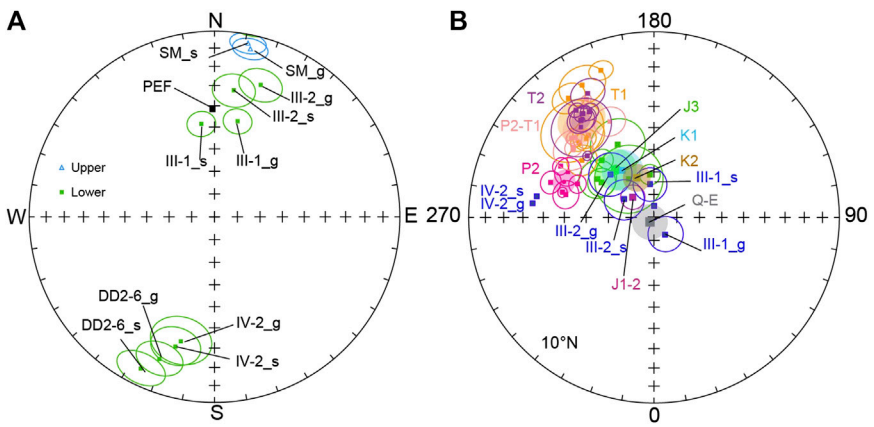

FIGURE 9 | (A) Equal-area projection of paleodirections in Zhaotong area (SM and DD2-6 from Liu et al., 2012) **(B)** Equal-area projections of the paleomagnetic poles generated in this study (blue square) and those of the Yangtze Block since Late Permian (Huang et al., 2008; 2018 and references therein). P_2, T_1/T_2, $J_1/J_2/J_3$, K_1/K_2, E, Q indicates Late Permian, Early/Late Triassic, Early/Middle/Late Jurassic, Early/Late Cretaceous, Eocene and Quaternary, respectively.

Besse, 2001), respectively. This indicates that the tilt-corrected paleodirections recorded in III-2 components were acquired during Early to Middle Jurassic while the III-2 *in-situ* directions were contemporary to Late Jurassic. If this is true, it confines the folding occurred during Early to Middle Jurassic. The most important folding event affecting the Yangtze platform during the Jurassic to Cretaceous periods was the Yanshanian Movement, which has a fold axis trending generally toward NNE-

NE (Yang et al., 1986). The flow dips at our sample locality have a north strike (eg, the strike of Xuanwei Formation sediments is 357°) and that fitting was suggested to have occurred during the Yanshanian Movement (Yang et al., 1986; Yan et al., 2003; Li et al., 2009; Dong et al., 2015). However, it is difficult to determine the timing of folding accurately. If the folding is earlier than the acquisition of the III-2 components, then the *in-situ* directions suggest Upper Jurassic remagnetization. Given these considerations, it is tentatively interpreted that the tilt-corrected directions were acquired prefolding (i.e., Early to Middle Jurassic), suggesting the Emeishan basalts of Unit III on this section experienced significant overprinting.

Mechanism of the Remagnetization

Native copper mineralization within the Emeishan flood basalts is present at many locations, but this is a highly localized and spatially discontinuous feature, being mainly restricted to unit IV. However, the occurrence of copper mineralization is not controlled by the distribution of the Emeishan basalts themselves, but mainly localized by faults and/or folds within basalt (Li et al., 2009; **Figure 1B**). At the studied section, two mining tunnels are in basalts flows at sites DD9 and DD10 in unit IV. Combined with the contamination of the unit IV paleomagnetic directions by a notable overprint, this suggests the lower unit IV basalts have experienced a remagnetization event associated with copper mineralization. However, the overlying basalt flows (DD2-6) as well as conglomerates, and other sections in this area preserve primary magnetizations (cf. Liu and Zhu, 2009; Liu et al., 2012). We speculate that the remagnetization of the Emeishan basalts is spatially related to copper mineralization and is a local phenomenon.

Another example of copper mineralization in massive volcanic rocks is in the Keweenaw Peninsula, United States, which contains large (~50 million tons) copper deposits hosted by ca. ~1.1 Ga mafic lavas and conglomerates (Halls and Palmer, 1981; Zhu et al., 2003). Geochemical studies reveal the copper associated within both Keweenawan rocks (Keweenaw Peninsula, Michigan, United States) and Emeishan basalts are related to low-temperature hydrothermal activity having assemblages of low-grade, secondary hydrothermal phases (Zhu et al., 2003; Li et al., 2005; Li et al., 2009; Wang et al., 2011). Remagnetization within the Keweenawan rocks has been demonstrated to be associated with the formation of native copper formation, with increasing degrees of overprinting moving west along the lava flow strikes (Halls and Pesonen, 1982). White (1978) proposed a model for the Keweenawan copper deposits where metamorphic fluids migrated up-dip along the strike and leached the copper from the host volcanic rocks. This model is consistent with the observation that the overprint of the host basalts was found to increase along strike coincident with an increase in burial metamorphism in the underlying Portage Lake Volcanic Group (Halls and Palmer, 1981; Palmer et al., 1981).

The remagnetization characteristics of the Emeishan basalts associated with copper mineralization are, however, different from those of Keweenawan rocks in at least two ways. First, the remagnetization is in rocks of an area of weak copper mineralization associated with the faults; and second, the location of remagnetization is stratabound by the copper mineralized flows. Additionally, the copper mineralization in the Emeishan basalts is mostly associated with bitumen and is dispersed (Halls and Palmer, 1981; Palmer et al., 1981; Zhu et al., 2003; Li et al., 2009). These differences are interpreted that the copper bearing hydrothermal fluids of the Emeishan basalts have a different origin than metamorphic fluids and that they probably migrated along the fault systems. Geochemical data suggest that native copper mineralization in the Emeishan basalts was a result of epigenetic hydrothermal activity associated with strong organic-inorganic interactions (Li et al., 2004; Wang et al., 2006; Li et al., 2009). The hydrothermal fluids are most likely due to basinal fluids that originally formed by meteoric waters (Li et al., 2009). These basin fluids migrated along the faults, leaching the Emeishan basalt flows and deposited copper in localized areas associated with fault systems. Compared to the extensive metamorphic fluids that concentrated copper in Keweenawan rocks, the basin fluids that leached the Emeishan basalts was probably inefficient over a much smaller scale.

Zeolite, bitumen and chlorite are present in the rocks of flow DD7. Microscopic investigation confirms the chlorite and zeolite within the DD7-22 samples. The higher chlorite content of flows DD7-22 when compared with flows DD2-6, suggests that DD7-22 experienced a higher degree of hydrothermal activity. This suggests that the remagnetization of the Emeishan basalt flows DD7-22 is due to the hydrothermal activity associated with copper mineralization. We suggest that the hydrothermal fluids migrated through the Emeishan basalts using the large tuff unit separating units III and IV of the basalts and the fault systems as pathways diverting laterally, reducing, but not stopping, the upward flow into unit IV. This would explain the reduction of the remagnetization signal moving up section. The main magnetic carrier of the DD7-22 basalt samples is (low-Ti) magnetite, which is suggested by the typical unblocking temperature. Thus, the magnetite within the DD7-22 samples is most probably autogenic and carries a chemical remanence magnetization due to the hydrothermal activity.

Many paleomagnetic studies in southwest China have demonstrated the effects of widespread remagnetizations (Kent et al., 1987; Dobson and Heller, 1992; Liu et al., 2011). Some ^{39}Ar-^{40}Ar data from whole-rock of basalt samples dating on the Emeishan basalts has yielded anomalously young ages at ~175, ~142, ~98 and ~42 Ma (Hou et al., 2002; Ali et al., 2004). The Longmenshan fault system to the north of the ELIP (**Figure 1A**), has been interpreted responsible for these overprint dates (Ali et al., 2004). The collision of the North and South China blocks, initially at the eastern end of Qinling Orogen in Late Permian to Early Triassic and suturing westward until the final suture occurred in the Early to Middle Jurassic (Zhao and Coe, 1987; Zhu et al., 1998; Yang and Besse, 2001), has been suggested as a potential cause of the older overprinting events (Ali et al., 2004). The ^{39}Ar-^{40}Ar ages of secondary basaltic minerals (eg, laumontite, actinolite) in the copper ores in NE Yunnan yield two age groups (226–228 Ma and 134–149.1 Ma; Zhu et al., 2005). Our paleomagnetic data suggest a significant remagnetization occurred during the Early to Middle Jurassic, which is consistent

with previous age estimates for mineralization. Considering that copper mineralization is widespread in Yunnan, Sichuan and Guizhou provinces (**Figure 1A**) and is associated with faults, the timing of formation of fault systems is probably coeval with mineralization. The faulting associated with the Yanshanian Movement in the opened up pathways for fluid migration through the Emeishan basalts, where copper was provided. This interpretation of paleomagnetic data is consistent with the suggestion that the main copper mineralization in this region is Jurassic (Li et al., 2009).

Implications to Future Study

Paleomagnetic studies on the Emeishan basalts report the prevalence of normal magnetizations over the presumably younger reversed polarity remanence (Huang and Opdyke, 1998; Ali et al., 2002; Liu et al., 2012). This study provides one explanation for this phenomenon in that parts of the Emeishan basalt unit IV of reverse polarity have been remagnetized during Early to Middle Jurassic. The steeper inclinations that characterize remagnetized sites suggest that caution should be exercised if similar steep inclinations are observed at other Emeishan flow sites, as these may be the result of remagnetization by younger hydrothermal activity. This observation may explain some previous results from the Emeishan basalts, for example, the directions observed in the study of Huang et al. (1986). The native copper deposits hosted in the Emeishan basalts are spatially associated with the remagnetization of the neighboring basalts flows. This process likely occurred in the Early to Middle Jurassic, which constrains the timing of copper mineralization to this period. The copper mineralization is generally small scale in volume and associated with local structure and lithology features. Paleomagnetic studies aiming to obtain primary remanent magnetizations should avoid such areas of the affected flood basalts. The high chlorite content of remagnetized basalts (DD21-03 and 10-10; **Figure 8**) identified in the microscopic investigation aided in the identification of remagnetized samples and future studies should include microscopic work. Future paleomagnetic studies in this region may provide further useful insights into the timing of copper mineralization, particularly in association with studies focusing on the Yanshanian Orogeny.

CONCLUSION

Stepwise thermal demagnetization on 176 basalt samples from 16 sites in the Dadi section from units III and IV of the Permian Emeishan basalt Formation yielded two distinct ChRMs. The samples in the upper unit IV have complicated magnetizations, with demagnetization behavior typical of extensive, but not complete remagnetization. These data yield a mean tilt-corrected direction of $D_s/I_s = 196.7^{\circ}/27.9^{\circ}$ ($n = 22$, $k_s = 50.1$, $\alpha_{95} = 9.6^{\circ}$) that most probably represents a primary remanence direction, but is likely contaminated by unresolved overprints that resulted from hydrothermal activity. The lower flows from unit III have been completely remagnetized, and yield a mean tilt corrected direction of $D_s/I_s = 8.8^{\circ}/31.6^{\circ}$ ($N = 9$, $k_s = 39.7$, $\alpha_{95} = 8.3^{\circ}$), which is of normal polarity and corresponds to a geomagnetic pole at 77.1°N, 240.0°E ($K_s = 49.2$, $A_{95} = 7.4^{\circ}$). The overprint directions have steeper inclinations (~19°) than the primary directions that have been successfully recovered from other sites.

By comparison with the Phanerozoic paleomagnetic poles of the South China Block, the inferred age of remagnetization time is likely the Early to Middle Jurassic. Field relationships reveal that the remagnetization of the Emeishan basalts is spatially related to copper mineralization and is likely to be associated with fluid migration through the fault systems. The remagnetization event related to copper mineralization is nevertheless a local phenomenon in the Emeishan basalts.

DATA AVAILABILITY STATEMENT

The raw data supporting the conclusions of this article will be made available by the authors, without undue reservation.

AUTHOR CONTRIBUTIONS

CY performed the study and measurements, SL assisted with fieldwork and measurements. All authors contributed to data analysis, interpretations and writing of the manuscript.

FUNDING

This study was supported by the National Natural Science Foundation of China and the Fundamental Research Funds for the Central Universities (lzujbky-2017-76). GAP acknowledges funding from a Natural Environment Research Council (NERC) Independent Research Fellowship (NE/P017266/1).

ACKNOWLEDGMENTS

We thank Lei Wang and Jiyun Yin for the help with sampling in the field, to Mingjian Cao for the help with the microscope investigation, to Randy Enkin for the PMGSC program. We are also grateful for the detailed review by Henry Halls, Jason Ali, John Geissman and two anonymous reviewers, and suggestions from James Tyburczy that help us improve the manuscript.

SUPPLEMENTARY MATERIAL

The Supplementary Material for this article can be found online at: https://www.frontiersin.org/articles/10.3389/feart.2020.590939/full#supplementary-material.

REFERENCES

Ali, J. R., Fitton, J. G., and Herzberg, C. (2010). Emeishan large igneous province (SW China) and the mantle-plume up-doming hypothesis. *J. Geol. Soc., London* 167 (5), 953–959. doi:10.1144/0016-76492009-129

Ali, J. R., Lo, C. H., Thompson, G. M., and Song, X. Y. (2004). Emeishan Basalt ^{40}Ar–^{39}Ar overprint ages define several tectonic events that affected the western yangtze platform in the mesozoic and cenozoic. *J. Asian Earth Sci.* 23 (2), 163–178. doi:10.1016/S1367-9120(03)00072-5

Ali, J. R., Thompson, G. M., Song, X. Y., and Wang, Y. L. (2002). Emeishan Basalts (SW China) and the 'end-guadalupian' crisis: magnetobiostratigraphic constraints. *J. Geol. Soc., London* 159, 21–29.

Ali, J. R., Thompson, G. M., Zhou, M. F., and Song, X. (2005). Emeishan large igneous province, SW China. *Lithos* 79 (3), 475–489. doi:10.1016/j.lithos.2004.09.013

Biggin, A. J., Strik, G. H. M. A., and Langereis, C. G. (2008). Evidence for a very-long-term trend in geomagnetic secular variation. *Nat. Geosci.* 1 (6), 395–398. doi:10.1038/ngeo181

Butler, R. F. (1992). *Paleomagnetism: Magnetic Domians to Geologic Terranes*. Boston: Blackwell Scientific Publications.

Courtillot, V., Jaupart, C., Manighetti, I., Tapponnier, P., and Besse, J. (1999). On causal links between flood basalts and continental breakup. *Earth Planet Sci. Lett.* 166 (3–4), 177–195. doi:10.1016/S0012-821X(98)00282-9

Day, R., Fuller, M., and Schmidt, V. (1977). Hysteresis properties of titanomagnetites: grain-size and compositional dependence. *Phys. Earth Planet. Inter.* 13 (4), 260–267. doi:10.1016/0031-9201(77)90108-X

Dobson, J. P., and Heller, F. (1992). Remagnetization in southeast China and the collision and suturing of the Huanan and Yangtze blocks. *Earth Planet Sci. Lett.* 111 (1), 11–21. doi:10.1016/0012-821X(92)90165-R

Dong, S., Zhang, Y., Zhang, F., Cui, J., Chen, X., Zhang, S., et al. (2015). Late jurassic–early cretaceous continental convergence and intracontinental orogenesis in east asia: a synthesis of the yanshan revolution. *J. Asian Earth Sci.* 114, 750–770. doi:10.1016/j.jseases.2015.08.011

Dunlop, D. J. (2002). Theory and application of the Day plot (Mrs/Ms versus Hcr/Hc), 1, Theoretical curves and tests using titanomagnetite data. *J. Geophys. Res.* 107.(B3) EPM 4-1–EPM 4-22 doi:10.1029/2001JB000486

Fisher, R. (1953). Dispersion on a sphere. *Proc. Roy. Soc. Lond. A* 217, 295–305. doi:10.1098/rspa.1953.0064

Halls, H. C., and Palmer, H. C. (1981). Remagnetization in keweenawan rocks. Part II: lava flows within the copper Harbor conglomerate, Michigan. *Can. J. Earth Sci.* 18 (9), 1395–1408. doi:10.1139/e81-131

Halls, H. C., and Pesonen, L. J. (1982). "Paleomagnetism of keweenawan rocks," in *Geology and tectonics of the lake superior basin*. Editors R. J. Wold and W. J. Hinze (Geol. Soc. Am. Mem., Press), 173–201.

He, B., Xu, Y. G., Chung, S. L., Xiao, L., and Wang, Y. (2003). Sedimentary evidence for a rapid, kilometer-scale crustal doming prior to the eruption of the Emeishan flood basalts. *Earth Planet Sci. Lett.* 213 (3–4), 391–405. doi:10.1016/S0012-821X(03)00323-6

He, B., Xu, Y. G., Huang, X. L., Luo, Z. Y., Shi, Y. R., Yang, Q. J., et al. (2007). Age and duration of the Emeishan flood volcanism, SW China: geochemistry and SHRIMP zircon U–Pb dating of silicic ignimbrites, post-volcanic Xuanwei Formation and clay tuff at the Chaotian section. *Earth Planet Sci. Lett.* 255 (3), 306–323. doi:10.1016/j.epsl.2006.12.021

Hou, Z. Q., Chen, W., and Lu, J. R. (2002). Collision event during 177–135 Ma on the eastern margin of the qinghai-Tibet plateau: evidence from $^{40}Ar/^{39}Ar$ dating for basalts on the western margin of the Yangtze platform. *Acta Geol. Sin.* 76 (2), 194–204.

Huang, B., Yan, Y., Piper, J. D. A., Zhang, D., Yi, Z., Yu, S., et al. (2018). Paleomagnetic constraints on the paleogeography of the east asian blocks during late paleozoic and early mesozoic times. *Earth Sci. Rev.* 186, 8–36. doi:10.1016/j.earscirev.2018.02.004

Huang, B., Zhou, Y. X., and Zhu, R. X. (2008). Discussions on phanerozoic evolution and formation of continental China, based on paleomagnetic studies Earth. *Sci. Front.* 15 (3), 348–359.

Huang, K. N., and Opdyke, N. D. (1998). Magnetostratigraphic investigations on an Emeishan basalt section in western Guizhou province, China. *Earth Planet Sci. Lett.* 163 (1–4), 1–14. doi:10.1016/S0012-821X(98)00169-1

Huang, K. N., Opdyke, N. D., and Kent, D. V. (1986). Further paleomagnetic results from permian Emeishan basalts in SW China chin. *Sci. Bull.* 2, 133–137. doi:10.1029/2010GC003267

Jones, C. H. (2002). User-driven integrated software lives: "Paleomag" paleomagnetics analysis on the Macintosh. *Comput. Geosci.* 28 (10), 1145–1151. doi:10.1016/S0098-3004(02)00032-8

Kent, D. V., Zeng, X. S., Zhang, W. Y., and Opdyke, N. D. (1987). Widespread late mesozoic to recent remagnetization of paleozoic and lower triassic sedimentary rocks from south China. *Tectonophysics* 139 (1–2), 133–143. doi:10.1016/0040-1951(87)90202-2

Kirschvink, J. L. (1980). The least-squares line and plane and the analysis of palaeomagnetic data. *Geophys. J. Roy. Astron. Soc.* 62 (3), 699–718. doi:10.1111/j.1365-246X.1980.tb02601.x

Kruiver, P. P., Dekkers, M. J., and Heslop, D. (2001). Quantification of magnetic coercivity components by the analysis of acquisition curves of isothermal remanent magnetisation. *Earth Planet Sci. Lett.* 189 (3–4), 269–276. doi:10.1016/S0012-821X(01)00367-3

Langereis, C., Haldan, M., and Biggin, A. J. (2012). Paleosecular variation during the permo-carboniferous reversed superchron: a comparison between the sedimentary and volcanic record. American Geophysical Union Fall Meeting Abstracts: GP11A-04.

Li, H., Mao, J., Chen, Y., Wang, D., Zhang, C., and Xu, H. (2005). "Epigenetic hydrothermal features of the Emeishan basalt copper mineralization in NE Yunnan, SW China," in *Mineral deposit research: meeting the global challenge*. Editors J. Mao and F. P. Bierlein (Berlin, Heidelberg: Springer), 149–152.

Li, H., Mao, J., Xu, Z., Chen, Y., Zhang, C., and Xu, H. (2004). Characteristics of copper mineralization distributed in huge Emeishan basalt district of northeast Yunnan province and west Guizhou province. *Acta Geol. Sin.* 25 (5), 495–502.

Li, H. M., Mao, J. W., Zhang, C. Q., Xu, H., Yan, S. H., and Gao, L. (2009). *Investigations on the copper mineralization hosted in the emeishan basalts in northeastern Yunnan province, China*. Beijing, China: Geology Publication House.

Li, Y., He, H., Ivanov, A. V., Demonterova, E. I., Pan, Y., Deng, C., et al. (2018). $^{40}Ar/^{39}Ar$ age of the onset of high-Ti phase of the Emeishan volcanism strengthens the link with the end-Guadalupian mass extinction. *Int. Geol. Rev.* 60 (15), 1906–1917. doi:10.1080/00206814.2017.1405748

Lin, J. L., Fuller, M., and Zhang, W. Y. (1985). Preliminary phanerozoic polar wander paths for the North and South China blocks. *Nature* 313, 444–449. doi:10.1038/313444a0

Liu, C., Ge, K., Zhang, C., Liu, Q., Deng, C., and Zhu, R. (2011). Nature of remagnetization of lower triassic red beds in southwestern China. *Geophys. J. Int.* 187, 1237–1249. doi:10.1111/j.1365-246X.2011.05196.x

Liu, C., Pan, Y., and Zhu, R. (2012). New paleomagnetic investigations of the Emeishan basalts in NE Yunnan, southwestern China: constraints on eruption history. *J. Asian Earth Sci.* 52 (0), 88–97. doi:10.1016/j.jseaes.2012.02.014

Liu, C. Y., and Zhu, R. X. (2009). Geodynamic significances of the Emeishan basalts. *Earth Sci. Front.* 16 (2), 52–69. doi:10.1016/S1872-5791(08)60082-2

Luo, W. J., Zhang, Z. C., Hou, T., and Wang, M. (2013). Geochronology-geochemistry of the cida bimodal intrusive complex, central Emeishan large igneous province, southwest China: petrogenesis and plume-lithosphere interaction. *Int. Geol. Rev.* 55 (1), 88–114. doi:10.1080/00206814.2012.689128

McElhinny, M. W., Embleton, B. J. J., Ma, X. H., and Zhang, Z. K. (1981). Fragmentation of asia in the permian. *Nature* 293 (5829), 212–216.

McFadden, P. L., and McElhinny, M. W. (1988). The combined analysis of remagnetization and direct observation in paleomagnetism. *Earth Planet Sci. Lett.* 87 (1), 161–172. doi:10.1016/0012-821X(88)90072-6

Palmer, H. C., Halls, H. C., and Pesonen, L. J. (1981). Remagnetization in Keweenawan rocks. Part I: conglomerates. *Can. J. Earth Sci.* 18 (3), 599–618. doi:10.1139/e81-053

Shellnutt, J. G., Denyszyn, S. W., and Mundil, R. (2012). Precise age determination of mafic and felsic intrusive rocks from the Permian Emeishan large igneous province (SW China). *Gondwana Res.* 22 (1), 118–126. doi:10.1016/j.gr.2011.10.009

Shellnutt, J. G., and Jahn, B. M. (2011). Origin of late permian Emeishan basaltic rocks from the panxi region (SW China): Implications for the Ti-classification and spatial–compositional distribution of the Emeishan flood basalts. *J. Volcanol. Geoth. Res.* 199 (1), 85–95. doi:10.1016/j.jvolgeores.2010.10.009

Tauxe, L., Robert, F. b., Rob, V. D. V., and Banerjee, S. K. (2010). *Essentials of paleomagnetism*. Berkerley, United States: University of California Press.

Van der Voo, R. (1990). The reliability of paleomagnetic data. *Tectonophysics* 184 (1), 1–9. doi:10.1016/0040-1951(90)90116-P

Van der Voo, R., Wu, F., Wang, Z. M., Dongwoo, S., Peacor, D. R., and Qizhong, L. (1993). Paleomagnetism and electron microscopy of the Emeishan basalts, Yunnan, China. *Tectonophysics* 221 (3–4), 367–379. doi:10.1016/0040-1951(93)90168-J

Wang, F. D., Zhu, X. Q., and Wang, Z. G. (2011). Madouzi-type (nodular) sedimentary copper deposit associated with the Emeishan basalt. *Sci. China Earth Sci.* 54 (12), 1880–1891.

Wang, X., Li, R., Cai, L. P., and Yang, J. (2010). Geological features, ore-forming conditions and prospecting potential of the Emeishan Basalt-hosted Cu deposits in the Sichuan-Yunnan-Guizhou border region. *Acta Geol. Sin.* 30, 174–182.

Wang, Y., Zhou, M. F., Qi, L., Hou, S., Gao, H., Zhang, Z., et al. (2006). The Zhaotong native copper deposit associated with the Permian Emeishan flood basalts, Yunnan, Southwest China. *Int. Geol. Rev.* 48, 742–753. doi:10.2747/0020-6814.48.8.742

Wang, Z. M., and Van der Voo, R. (1993). Rapid apparent polar wandering of South China during the latest paleozoic and early mesozoic: a paleomagnetic study of Upper Permian limestones from Guizhou province. *Tectonophysics* 222 (2), 165–176. doi:10.1016/0040-1951(93)90047-N

Wei, C., and Powell, R. (2003). Phase relations in high-pressure metapelites in the system KFMASH (K2O–FeO–MgO–Al2O3–SiO2–H2O) with application to natural rocks. *Contrib. Mineral. Petrol.* 145 (3), 301–315.

White, W. S. (1978). A theoretical basis for exploration for native copper in northern Wisconsin. *Geol. Surv. Circular* 769, 19. doi:10.3133/cir769

Xu, Y., Chung, S. L., Jahn, B., and Wu, G. (2001). Petrologic and geochemical constraints on the petrogenesis of permian-triassic Emeishan flood basalts in southwestern China. *Lithos* 58 (3-4), 145–168. doi:10.1016/S0024-4937(01)00055-X

Xu, Y. G., He, B., Chuang, S. L., Frey, F. A., and Menzies, M. A. (2004). Geologic, geochemical, and geophysical consequences of plume involvement in the Emeishan floodabasalt province. *Geology* 32 (10), 917–920. doi:10.1130/G20602.1

Yan, D. P., Zhou, M. F., Song, H. L., Wang, X. W., and Malpas, J. (2003). Origin and tectonic significance of a mesozoic multi-layer over-thrust system within the Yangtze block (South China). *Tectonophysics* 361 (3–4), 239–254. doi:10.1016/S0040-1951(02)00646-7

Yan, D., Zhang, L., and Qiu, Z. (2013). Carbon and sulfur isotopic fluctuations associated with the end-Guadalupian mass extinction in South China. *Gondwana Res.* 24 (3–4), 1276–1282. doi:10.1016/j.gr.2013.02.008

Yang, Z., and Besse, J. (2001). New esozoic apparent polar wander path for south China: tectonic consequences. *J. Geophys. Res.* 106 (B5), 8493–8520. doi:10.1029/2000JB900338

Yang, Z. Y., Cheng, Y. Q., and Wang, H. Z. (1986). *The geology of China*. Oxford, England: Clarendon Press.

Yunnan Bureau (1989). *Encyclopedia of the geology of Yunnan province*. Beijing, China: Geological Publication House.

Zhao, X. X., and Coe, R. S. (1987). Paleomagnetic constraints on the collision of and rotation of North and South China. *Nature* 327, 141–144.

Zheng, L., Yang, Z., Tong, Y., and Yuan, W. (2010). Magnetostratigraphic constraints on two-stage eruptions of the Emeishan continental flood basalts. *Geochem. Geophys. Geosyst.* 11 (12), Q12014. doi:10.1029/2010GC003267

Zhu, B. Q., Dai, T. M., Yao-Guo, H. U., Zhang, Z. W., Chen, G. H., Peng, J. H., et al. (2005). 40Ar/39Ar and U-Th-Pb dating for native copper mineralizations of two stages from the Emeishan flood basalts in northeastern Yunnan province, China. *Geochimica* 34, 235–247.

Zhu, B. Q., Hu, Y. G., Zhang, Z. W., and Chang, X. Y. (2003). Discovery of the copper deposits with features of the Keweenawan type in the border area of Yunnan and Guizhou provinces. *Sci. China Earth Sci.* 46 (1), 60–72.

Zhu, R. X., Yang, Z. Y., and Wu, H. N. (1998). Preliminary phanerozoic polar wander paths and movements for the main Chinese blocks. *Chin. Sci. Bull.* 28, 1–16.

Zijderveld, J. (1967). "AC demagnetization of rocks: analysis of results," in *Methods in paleomagnetism*. Editors D. W. Collison, K. M. Creer, and S. K. Runcorn. (New York, NY: Elsevier), 245–286.

Conflict of Interest: The authors declare that the research was conducted in the absence of any commercial or financial relationships that could be construed as a potential conflict of interest.